ADVANCES IN ATMOSPHERIC SCIENCES, VOL. 38, APRIL 2021, 555–568

• **Original Paper** •

Distinctive MJO Activity during the Boreal Winter of the 2015/16 Super El Niño in Comparison with Other Super El Niño Events

Xuben LEI, Wenjun ZHANG*, Pang-Chi HSU, and Chao LIU

Key Laboratory of Meteorological Disaster, Ministry of Education/Joint International Research Laboratory of Climate and Environmental Change/Collaborative Innovation Center on Forecast and Evaluation of Meteorological Disasters, Nanjing University of Information Science & Technology, Nanjing 210044, *China*

(Received 3 August 2020; revised 21 November 2020; accepted 10 December 2020)

ABSTRACT

Many previous studies have demonstrated that the boreal winters of super El Niño events are usually accompanied by severely suppressed Madden-Julian oscillation (MJO) activity over the western Pacific due to strong descending motion associated with a weakened Walker Circulation. However, the boreal winter of the 2015/16 super El Niño event is concurrent with enhanced MJO activity over the western Pacific despite its sea surface temperature anomaly (SSTA) magnitude over the Niño 3.4 region being comparable to the SSTA magnitudes of the two former super El Niño events (i.e., 1982/83 and 1997/98). This study suggests that the MJO enhanced over western Pacific during the 2015/16 super El Niño event is mainly related to its distinctive SSTA structure and associated background thermodynamic conditions. In comparison with the previous super El Niño events, the warming SSTA center of the 2015/16 super El Niño is located further westward, and a strong cold SSTA is not detected in the western Pacific. Accordingly, the low-level moisture and air temperature (as well as the moist static energy, MSE) tend to increase in the central-western Pacific. In contrast, the low-level moisture and MSE show negative anomalies over the western Pacific during the previous super El Niño events. As the MJO-related horizontal wind anomalies contribute to the further westward warm SST-induced positive moisture and MSE anomalies over the western tropical Pacific in the boreal winter of 2015/16, stronger moisture convergence and MSE advection are generated over the western Pacific and lead to the enhancement of MJO convection.

Key words: super El Niño, Madden-Julian oscillation, moisture diagnosis

Citation: Lei, X. B., W. J. Zhang, P.-C. Hsu, and C. Liu, 2021: Distinctive MJO activity during the boreal winter of the 2015/16 Super El Niño in comparison with other super El Niño events. *Adv. Atmos. Sci.*, **38**(4), 555–568, https://doi.org/10.1007/s00376-020-0261-x.

Article Highlights:

- The western Pacific MJO is abnormally active during the 2015/16 super El Niño winter compared to weak MJO conditions in the 1982/83 and 1997/98 super El Niño boreal winters.
- The warm SSTA of the 2015/16 super El Niño event is extended westward when compared to previous super El Niño events, providing sufficient moisture/MSE for MJO development.

1. Introduction

The Madden-Julian oscillation (MJO, Madden and Julian, 1971) is the most significant mode of atmospheric intraseasonal variability over the tropics. The MJO usually initiates over the western Indian Ocean, slowly propagates eastward through the Maritime Continent to the central Pacific, and dissipates near the dateline (Madden and Julian, 1972). MJO-related circulations/convection and heating anomalies can influence various weather events and climate variability, such as tropical cyclone activity (Liebmann et al., 1994; Camargo et al., 2009), monsoons (Yasunari, 1979; Li et al., 2018), mid-latitude storm tracks (Zheng et al., 2018), and the North Atlantic oscillation (Cassou, 2008).

Significant progress has been made over the past few decades in revealing the basic features and underlying physical mechanisms of the MJO (e.g., Weickmann et al., 1985; Ferranti et al., 1990; Sperber, 2003; Kiladis et al., 2005). Previous studies have emphasized the importance of moisture processes and associated moist static energy (MSE) in the initiation, propagation, and intensity of the MJO (Kemball-Cook and Weare, 2001; Maloney, 2009; Andersen and Kuang, 2012; Adames and Wallace, 2014; Pritchard and

* Corresponding author: Wenjun ZHANG
Email: zhangwj@nuist.edu.cn

Bretherton, 2014). For example, the horizontal transportation of moisture/MSE plays a crucial role in both the initiation (Zhao et al., 2013; Maloney and Wolding, 2015) and development (Andersen and Kuang, 2012; Adames and Wallace, 2014) of MJO-related convection. The low-level moistening ahead of the MJO convection results in a relatively unstable stratification that favors the eastward development of the deep convection (Hsu and Li, 2012; Kim et al., 2014).

The El Niño–Southern Oscillation (ENSO) is the most dominant coupled ocean–atmosphere phenomenon on the interannual timescale. Numerous studies have demonstrated its significant influences on global climate, mostly through so-called atmospheric bridge mechanisms (e.g., Bjerknes, 1969; Wallace et al., 1998; Alexander et al., 2002; Lau and Nath, 2006; Zhang et al., 2015). The relationship of ENSO with the MJO has also been largely documented. Observations show that El Niño events are usually accompanied by active and continuous eastward-propagating MJO events (Kessler et al., 1995; Zhang and Gottschalck, 2002; Zavala-Garay et al., 2005). In the spring and summer of years with developing El Niño events, the intraseasonal zonal westerly winds associated with the active MJO can force an eastward extension of the tropical Pacific warm pool edge, and thus contribute to warming sea surface temperature (SST) anomalies (SSTAs) in the central to eastern tropical Pacific (Vecchi and Harrison, 2000; Hendon et al., 2007; Tang and Yu, 2008).

El Niño is also able to influence initiation, intensity, propagation, and other basic characteristics of the MJO by modulating the SST distribution (Kim et al., 2010; Kapur and Zhang, 2012; Wang et al., 2019). During the mature and decaying phases of El Niño, MJO intensity is normally weakened in the western tropical Pacific (Chen et al., 2015). The frequency of intraseasonal oscillation is higher over the western Pacific, and mainly characterized by northwestward propagation during decaying El Niño events in summer (Liu et al., 2016a). Correspondingly, the eastward propagation of the MJO is also weakened at the equator (Lin and Li, 2008). Roughly opposite responses of the MJO can be found for La Niña events. In recent years, another type of El Niño event has occurred much more frequently with a maximum SSTA center located in the central Pacific (CP) (Larkin and Harrison, 2005; Ashok et al., 2009; Kao and Yu, 2009; Kug et al., 2009; Ren and Jin, 2011; Zhang et al., 2014). In contrast to traditional El Niño events, the CP El Niño is usually accompanied by enhanced MJO activity and further eastward propagation during its mature and decaying phases (e.g., Gushchina and Dewitte, 2012; Feng et al., 2015; Chen et al., 2016; Hsu and Xiao, 2017).

Among El Niño events, so-called super El Niño events have extremely warm SSTAs in the tropical Pacific and are of considerable public concern since they can lead to more severe global catastrophic disasters compared to normal El Niño events (Smith et al., 1999; Zhang et al., 2016; Geng et al., 2017). Since the late 1970s when satellite observation began, three super El Niño events (i.e., 1982/83, 1997/98, and 2015/16) have been well-observed. These three events share similar characteristics in terms of evolution and intensity, and exhibit similar MJO-associated westerly wind anomalies during their development stages (McPhaden, 1999; Levine and McPhaden, 2016; Chen et al., 2017). However, the 2015/16 super El Niño event does exhibit some unique characteristics and climate impacts compared to the two prior super El Niño events (Jacox et al., 2016; L'Heureux et al., 2017; Paek et al., 2017; Lyu et al., 2018). Considering the different oceanic/atmospheric features of the 2015/16 super El Niño event, some MJO features during its mature phase may also differ from the other two super El Niño events. We observe that the 2015/16 super El Niño event coincides with enhanced MJO activity over the western Pacific, which is very different from the previous super El Niño events. This observation deserves further investigation in order to understand the possible reasons for this uniqueness during the boreal winter of the 2015/16 super El Niño event.

In this study, we analyze the differences in MJO activity of the 2015/16 super El Niño event compared to the previous two super El Niño events. Possible physical reasons for the unique MJO feature of the 2015/16 super El Niño event are further investigated based on the diagnoses of moisture and MSE budget equations. First, the data and methodology used in this study are described in section 2. Then, the distinct MJO feature associated with the 2015/16 super El Niño event is displayed through inter-comparison with the other two super El Niño events in section 3. Possible reasons for the unique MJO activity during the 2015/16 El Niño are examined in section 4. Finally, conclusions and discussions are summarized in section 5.

2. Data and methodology

2.1. *Datasets*

In this study, daily mean outgoing longwave radiation data (OLR, Liebmann and Smith, 1996) and monthly global gridded precipitation data (Xie and Arkin, 1997) with horizontal resolution of 2.5° × 2.5° from the National Oceanic and Atmospheric Administration (NOAA) are used to identify convective activity at the intraseasonal and interannual timescales, respectively. Monthly SST data with horizontal resolution of 1° × 1° is obtained from the Hadley Centre Sea Ice and Sea Surface Temperature datasets (HadISST1; Rayner et al., 2003). To understand the physical processes related to MJO development, the three-dimensional dynamic and thermodynamic fields, including daily averaged horizontal winds, vertical pressure velocity, air temperature, specific humidity, and geopotential height, are collected from the European Centre for Medium-Range Weather Forecasts (ECMWF) interim reanalysis (ERA-Interim, Dee et al., 2011). The sensible heat flux (SHF), latent heat flux (LHF), and longwave (LW) and shortwave (SW) radiation fluxes at the bottom and top of the atmosphere from the ERA-Interim reanalysis are also used. The horizontal resolution of all ERA-Interim datasets is 1.5° × 1.5°. We also use the all-season real-time multivariate MJO

(RMM) index (Wheeler and Hendon, 2004; http://www.bom.gov.au/climate/mjo/graphics/rmm.74toRealtime.txt) to examine the MJO amplitude over the tropics.

2.2. *Methodology*

To extract the MJO-associated intraseasonal variability (30–90 days), a 201-point Lanczos bandpass filter is used (Duchon, 1979). The monthly mean amplitude of the MJO is measured as the square root of the filtered OLR variance within a 3-month running window centered on that calendar month (Hendon et al., 2007). Niño3.4 index is used for defining a super El Niño event as the intensity of El Niño, which is calculated by the standardized area-averaged SSTA in the Niño3.4 region (5°S–5°N, 120°–170°W), and the Niño3.4 index during the mature phase of super El Niño events is usually above the 2 standard deviations. Anomalies were calculated as the departures from the climatological average over the entire study period (1979–2018). The monthly RMM amplitude is calculated by following steps: first calculate the 90 days running averaged of daily RMM amplitude [$(RMM1^2+RMM2^2)^{1/2}$], and then calculate the monthly mean RMM amplitude of every single month.

Column-integrated MSE and low-level moisture are important factors for the development and maintenance of the MJO (Maloney, 2009; Hsu and Li, 2012; Sobel and Maloney, 2013; Adames and Wallace, 2014; Kim et al., 2014). The moisture and MSE budget terms are diagnosed to understand the key processes contributing to the distinct MJO activity in the boreal winter of 2015/16. The moisture budget equation at the intraseasonal timescale is based on Eq. (1) (Yanai et al., 1973):

$$\left(\frac{\partial q}{\partial t}\right)' = -(V\cdot\nabla q)' - \left(\omega\frac{\partial q}{\partial p}\right)' - \left(\frac{Q_2}{L}\right)', \quad (1)$$

where q is the specific humidity, and V and ω represent horizontal wind and vertical pressure velocity, respectively. Q_2 and L denote the apparent moisture sink and latent heat of condensation, and Q_2/L is regarded as a residual of the moisture budget. Prime notation indicates the intraseasonal (30–90 day) component. Here, the vertical integral of Eq. (1) is calculated from 1000 hPa to 700 hPa, considering that low-level moisture plays a key role in development of the MJO.

The MSE budget at intraseasonal timescales is defined by Eq. (2) (Neelin and Held, 1987):

$$\left(\frac{\partial m}{\partial t}\right)' = -(V\cdot\nabla m)' - \left(\omega\frac{\partial m}{\partial p}\right)' + \mathrm{LHF}' + \mathrm{SHF}' + \mathrm{LW}' + \mathrm{SW}', \quad (2)$$

where m denotes MSE, defined by $m = C_pT+Lq+gz$, and C_p is the heat capacity of dry air at constant pressure (1004 J K^{-1} kg^{-1}), L is the specific latent heat for a unit substance (2.5×10^6 J kg^{-1}), g is the gravitational constant (9.8 m s^{-2}), and z is geopotential height. The left-hand term and first two terms of the right-hand side of Eq. (2) are vertically integrated from 1000 hPa to 100 hPa. The net heat flux terms are calculated as the differences between the top and surface level of the atmosphere.

3. Distinct MJO activity during the 2015/16 super El Niño

Figure 1a shows the Niño3.4 index evolutions for the three super El Niño events. With the exception of some differences at the developing and decaying stages, the general evolutions and magnitudes are quite similar for these three events. The magnitude of the 2015/16 super El Niño event

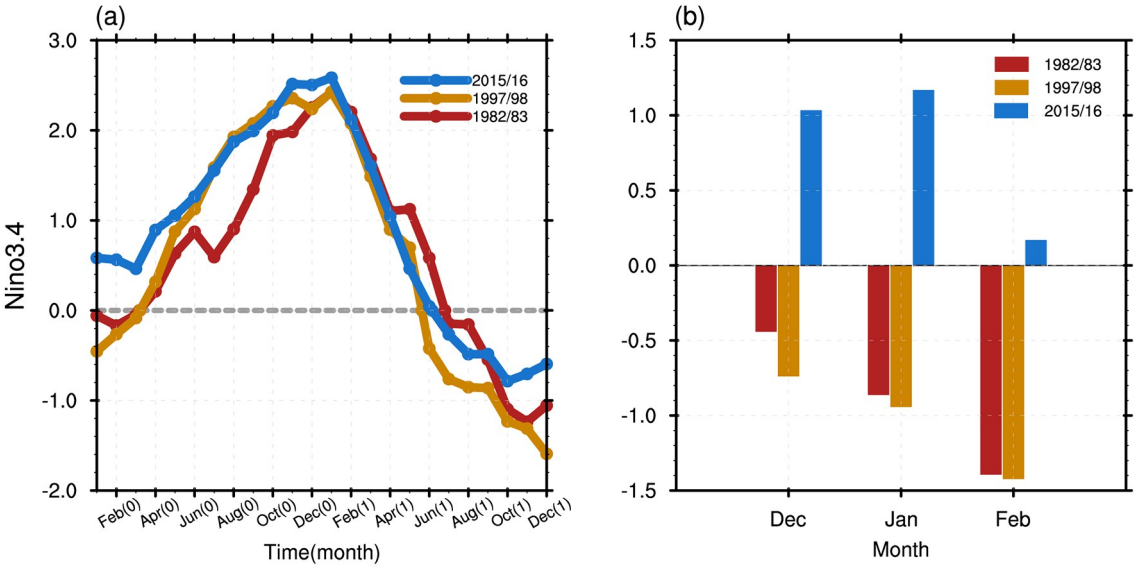

Fig. 1. (a) Time evolutions of the Niño3.4 index (°C) for 1982/83 (red), 1997/98 (orange) and 2015/16 (blue) events relative to the climatological state in 1979–2018. Notation of 0 (1) in parentheses on the x-axis represents the El Niño developing (decaying) year. (b) Anomalies of monthly RMM index amplitude in the boreal winters of three super El Niño events.

is slightly larger, relative to the other two super El Niño events during their respective peak seasons. To display the MJO intensity during each of the three super El Niño events, the amplitudes of the RMM index during their boreal winters (during which the MJO and ENSO signals are the most vigorous) are shown in Fig. 1b. Consistent with previous studies (e.g., Gushchina and Dewitte, 2012; Chen et al., 2016; Wang et al., 2018), overall MJO activity is strongly suppressed during boreal winters of the 1982/83 and 1997/98 super El Niño events. In contrast, the 2015/16 super El Niño event exhibits a very different MJO response with enhanced MJO activity during boreal winter. From the phase space diagram of the MJO (Fig. 2a) during boreal winters of the three super El Niño events, the eastward propagation of the MJO during 2015/16 is clearly more robust and of obviously higher amplitude over the Maritime Continent compared to the central-western Pacific area. In contrast, the MJO intensity over the Indian Ocean (phases 1–3) is nearly comparable for the three super El Niño events. The monthly averaged RMM amplitude anomalies (Fig. 1b) represents the overall states of the MJO in the equatorial region for each of the three super El Niño events. To reveal the geographical distribution of MJO activity and quantify the contributions of frequency effect and magnitude effect to the distinct MJO enhancement during 2015/16, we compare the frequency of active MJO days (RMM amplitude greater than 1) and the averaged amplitude for each phase during boreal winters between the three super El Niño events (Figs. 2b and 2c). Instances of an active MJO were more frequent in phases 4–7 (especially phase 4) during the boreal winter of

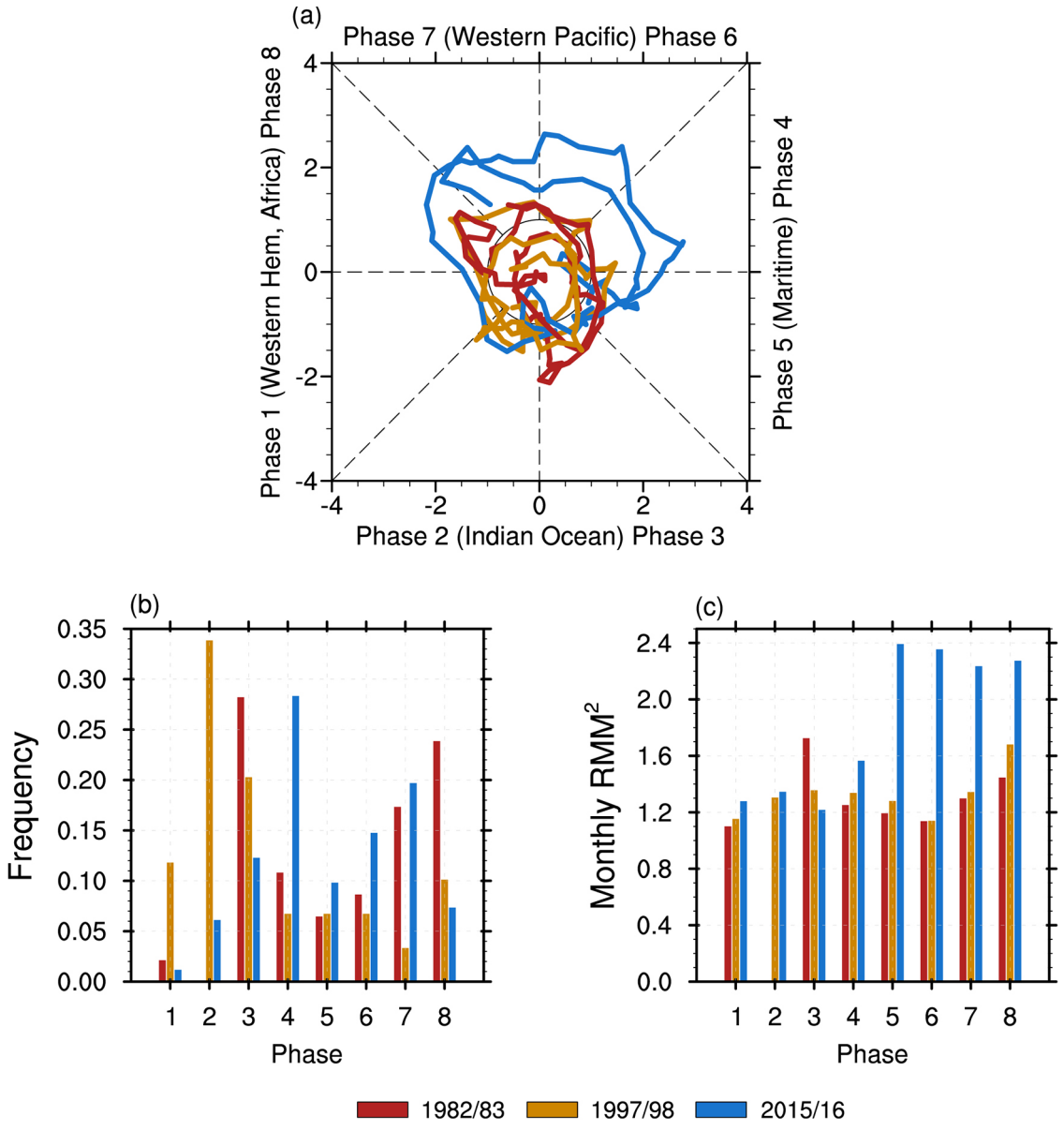

Fig. 2. (a) MJO phase space diagrams for the boreal winters of 1982/83 (red), 1997/98 (yellow), and 2015/16 (blue). (b) The frequency of each MJO phase during the boreal winters of 1982/83, 1997/98, and 2015/16. (c) Same as (b) but for the MJO intensity.

2015/16, while they were less frequent in other phases (phases 1–3 and 8) when compared to the boreal winters of 1982/83 and 1997/98 (Fig. 2b). The active MJO over the Maritime Continent and Pacific area (phases 4–8) also had a stronger amplitude during 2015/16 than during the previous two events (Fig. 2c). Thus, the most significant enhancement of MJO activity during 2015/16 occurred over the Maritime Continent to western Pacific (phases 5–8), where the MJO was more active in terms of amplitude and frequency.

To clearly identify the key region with significant MJO changes associated with super El Niño events, Figure 3 shows the spatial patterns of the MJO-related (30–90 day filtered) convection variability. For the 1982/83 and 1997/98 super El Niño events, the MJO intensity is significantly suppressed over most of the tropical Indo-Pacific region (Figs. 3a, b). A slightly weakened MJO can also be seen in the tropical Indian Ocean during the boreal winter of the 2015/16 super El Niño, while the MJO is remarkably strengthened over the Maritime Continent and the tropical western Pacific of the Southern Hemisphere (Fig. 3c), which is consistent with the results shown in Fig. 2. The enhanced MJO activity during the 2015/16 super El Niño event experienced a maximum over the western Pacific near 10°S, which is climatologically the region with the most vigorous MJO activity. Previous studies have also found similar intraseasonal variability with this enhanced activity (Liu et al., 2016b). The unique change in MJO amplitude during boreal winter of the 2015/16 super El Niño event can also be clearly seen when the difference is taken between it and the previous two super El Niño events (Figs. 3d–f). The remarkable enhancement of MJO intensity during the 2015/16 super El Niño event is observed more consistently over the tropical western Pacific (green boxes in Fig. 3, 120°–170°E, 5°–15°S) relative to the 1982/83 super El Niño event (Fig. 3d), the 1997/98 super El Niño event (Fig. 3e), and their average (Fig. 3f). This region will be our focus since the largest difference appears here.

Considering modulation of the background oceanic-atmospheric conditions on MJO activity, Figure 4 displays anomalous SST and precipitation patterns associated with the boreal winters of three super El Niño events. All three events are characterized by extremely warm SSTAs and above average precipitation over the central to eastern tropical Pacific. Compared to the previous two super El Niño events, the warm SSTA center is clearly displaced westward by about 20 degrees of longitude for the 2015/16 super El Niño event (Figs. 4a–c). This observation is further supported by the SSTA difference between the 2015/16 case and the average of the other two cases (Fig. 4d). Figure 4d also shows that the precipitation anomalies are stronger in the central Pacific and weaker in the eastern Pacific during the 2015/16 boreal winter compared to the other two cases. In the western Pacific, negative SSTAs and reduced precipitation are evident for the boreal winters of the 1982/83 and 1997/98 super El Niño events (Figs. 4a, b). However, slightly negative SSTAs can be found in the western Pacific with very small negative precipitation anomalies during the boreal winter of 2015/16 (Fig. 4c). These observations suggest that the distinct oceanic and atmospheric anomalies in the western Pacific during the boreal winter of the 2015/16 super El Niño event (Fig. 4d) provide different background conditions for MJO activity and may possibly lead to unique MJO anomalies in contrast to the previous super El Niño events. The possible effects of the background conditions will be investigated in detail in the next section.

4. Possible mechanisms responsible for enhanced MJO activity during the boreal winter of 2015/16

The development of MJO convection is closely linked with the low-level moisture and MSE since these factors are providing the favorable preconditioning for the convection. (Maloney, 2009; Andersen and Kuang, 2012; Hsu and Li,

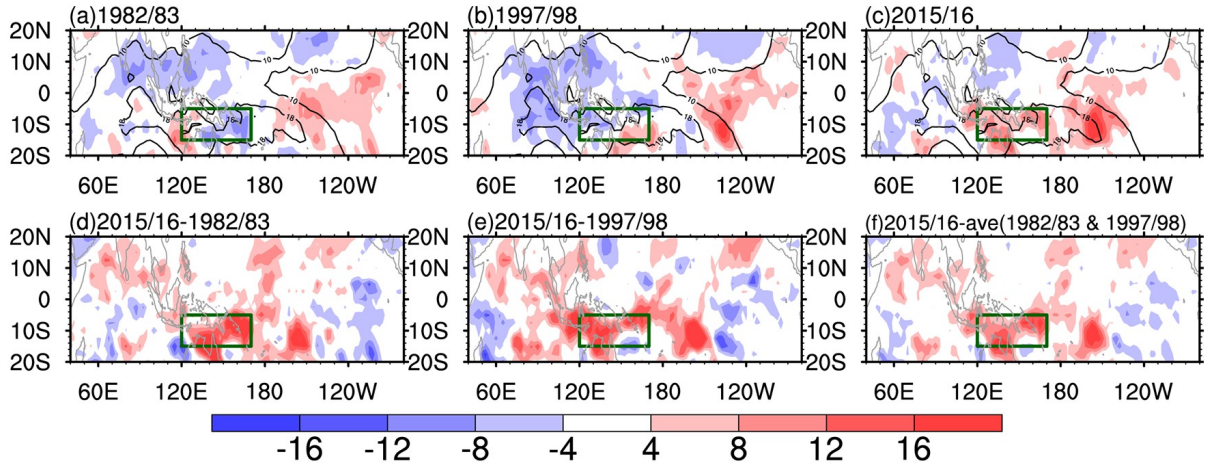

Fig. 3. Anomalous distributions of 30–90 d filtered OLR standard deviation (shading, W m^{-2}) during the boreal winters of (a) 1982/83, (b) 1997/98, and (c) 2015/16, superimposed on the climatology (contours, W m^{-2}). The corresponding differences between (d) 2015/16 minus 1982/83, (e) 2015/16 minus 1997/98, (f) 2015/16 minus the average of 1982/83 and 1997/98.

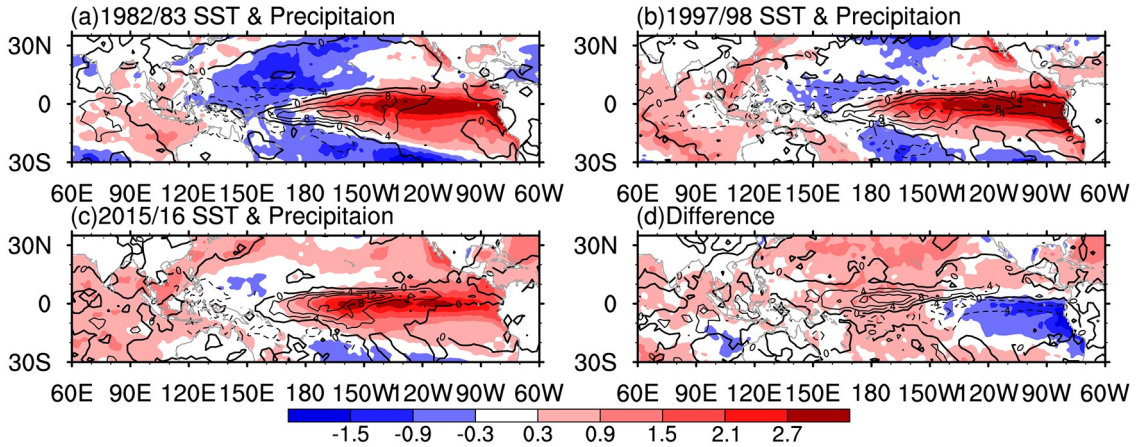

Fig. 4. Seasonal SST (shading, °C) and precipitation (contours, mm d^{-1}) anomalies in the boreal winters of (a) 1982/83, (b) 1997/98, and (c) 2015/16. (d) Their differences between 2015/16 and the average of 1997/98 and 1982/83.

2012; Kim et al., 2014). We diagnose the low-level moisture budget, Eq. (1), and the column-integrated MSE budget, Eq. (2), over the western tropical Pacific (5°–15°S, 120°–170°E, the green box in Fig. 3) to investigate key processes causing unique MJO activity during the boreal winter of 2015/16.

Composite OLR anomalies at the intraseasonal timescale are used to represent local MJO evolution in the western Pacific. Active MJO events were selected for the composite when the 30–90 day filtered OLR over the western Pacific was greater than 1 standard deviation. The date with the minimum 30–90 day OLR is defined as day 0. As shown in Fig. 5a, the OLR anomalies change their signs from positive to negative around day -10, when the MJO convective signal initiates and develops. For low-level moisture, its maximum tendency also occurs around day -10, leading the MJO convection maximum by about 10 days (Fig. 5b). The phase relationship between the MJO-related convection and moisture suggests an important effect of the leading low-level moisture accumulation on the growth of the MJO convection. Despite similar evolutions of MJO convection and moisture anomalies for all three super El Niño events, the amplitude of moisture tendency in the 2015/16 event is about twice as strong as those of the 1982/83 and 1997/98 events (Figs. 5a, b). The enhanced moisture tendency is likely contributing to the strong amplitude of MJO convection in the 2015/16 event (Fig. 5a) during its development stage (from day –10 to 0, when the OLR ranges from zero to its minimum). Focusing on the MJO development period, the moisture tendency is positive and the vertical moisture advection shows a large contribution. Although the horizontal moisture advection is in phase with the moisture tendency, it has a relatively small contribution compared to vertical advection and latent heating processes during the MJO development stage (Figs. 5c–d). Note that the moisture begins discharging through apparent moisture sinking and latent heat of condensation when the MJO convection is established, which is represented as Q_2/L in Eq. (1) (Kemball-Cook and Weare, 2001; Kiladis et al., 2005).

Figure 6 further compares the moisture budget terms and the contributions of scale interactions to the key processes during day −10 to day 0, when MJO convection grows quickly. During the developing stage of MJO convection, the moisture tendency ($\partial q'/\partial t$) of the 2015/16 event is much stronger than those of the 1982/83 and 1997/98 events, which comes mainly from vertical moisture advection, consistent with the results shown in Fig. 5. According to the continuity equation, the vertical advection term (the second term on the right-hand side of Eq. (1)) can be further decomposed as follows:

$$-\left(\omega\frac{\partial q}{\partial p}\right)' = -(q\cdot\nabla V)' - \left(\frac{\partial(\omega q)}{\partial p}\right)', \tag{3}$$

where the right-hand side terms represent horizontal moisture convergence and vertical moisture flux convergence, respectively. To elucidate the importance of scale interactions for vertical moisture advection, q and V are decomposed into low-frequency background state (LFBS, longer than 90 days), intraseasonal component (30–90 days), and higher-frequency disturbances (less than 30 days) as depicted in the following equation:

$$q = \overline{q} + q' + q^*; V = \overline{V} + V' + V^* . \tag{4}$$

The overbar, prime, and asterisk indicate LFBS, intraseasonal, and higher-frequency components, respectively. Based on this, the zonal moist convergence can be separated into 9 terms representing the interactions between different timescales:

$$\begin{aligned}\omega\frac{\partial q}{\partial p} =& \overline{q}\cdot\nabla\overline{V} + \overline{q}\cdot\nabla V' + \overline{q}\cdot\nabla V^* + q'\cdot\nabla\overline{V} + \\ & q'\cdot\nabla V' + q'\cdot\nabla V^* + \\ & q^*\cdot\nabla\overline{V} + q^*\cdot\nabla V' + q^*\cdot\nabla V^* + \frac{\partial(\omega q)}{\partial p} .\end{aligned} \tag{5}$$

The diagnostic result of Eq. (5) shows that the El Niño-related LFBS moisture converged by the MJO-related hori-

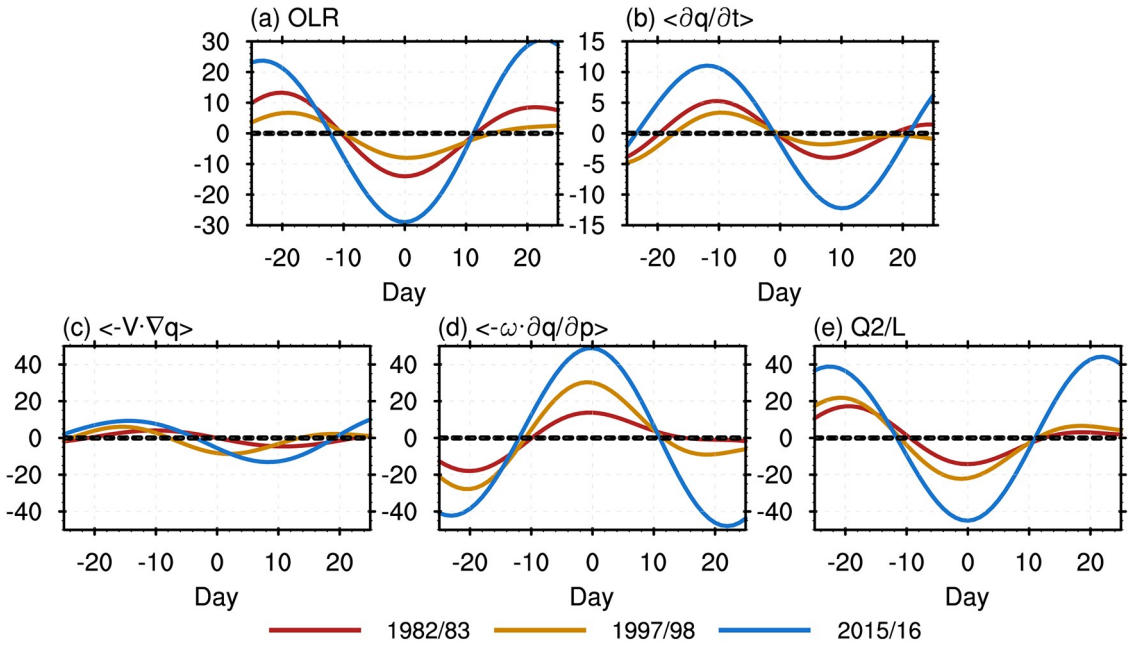

Fig. 5. Composites of (a) 30–90 day filtered OLR anomaly (W m^{-2}) averaged over the western Pacific region (120°–170°E, 5°–15°S) with day 0 as the occurrence of maximum MJO OLR anomaly. The blue, orange and red lines represent MJO evolutions during the boreal winters of 2015/16, 1997/98 and 1982/83, respectively. (b–e) Same as (a) except for column-integrated (1000–700 hPa) intraseasonal moisture budget terms (10^{-6} kg m^{-2} s^{-1}) for (b) moisture tendency, (c) horizontal advection, (d) vertical advection, and (e) residual of the moisture budget.

zontal wind anomalies $(\overline{q}\cdot\nabla V')'$ is dominantly responsible for the different growth rates of the low-level moisture tendency and MJO convection amplitude associated with the three super El Niño events, which means leading planetary boundary layer moisture convergence is an important factor for the development of MJO convection (Wang, 1988). It suggests that sufficient LFBS water vapor provides an important background condition for the enhanced vertical moisture advection associated with the MJO during the boreal winter of 2015/16. In comparison, contributions from other terms are relatively negligible (Fig. 6b).

Figure 7 shows the distributions of LFBS moisture ($\overline{q}$) and intraseasonal horizontal wind (V') during the development stage of MJO convection. In the boreal winters of 1982/83 and 1997/98, below than average moisture occurs over most regions of the western tropical Pacific, while above than average moisture covers the eastern equatorial Pacific (Figs. 7a, b). During the MJO development stage, the easterly and westerly wind anomalies prevail, respectively, over the eastern and western edge of the western Pacific (120°–170°E) for both the 1982/83 and 1997/98 cases. Compared to 1982/83 and 1997/98, positive moisture anomalies are observed over the western equatorial Pacific during the boreal winter of 2015/16 (Figs. 7c, d), accompanied by a remarkably westward shift of warm SSTAs (Figs. 4c, d). Therefore, the MJO-related wind anomalies can transport a moister atmosphere from the adjacent ocean toward the western Pacific and moisten the low-level atmosphere there, contributing positively to MJO convective development in the boreal winter of 2015/16 (Fig. 7c).

In addition to the preconditioning effect of low-level moisture, the positive MSE anomalies associated with the MJO are also argued to be important for the initiation and growth of MJO convection (e.g., Maloney, 2009; Andersen and Kuang, 2012; Zhao et al., 2013; Maloney and Wolding, 2015; Hsu and Xiao, 2017). Although the MSE variability is dominated by the moisture change at the MJO timescale (Maloney, 2009), its budget diagnosis, shown in Eq. (2), could provide additional insights about the effects of radiative heating and surface fluxes on the MJO evolution. We analyze the MSE evolution and its related physical processes for MJO initiation and development during the three super El Niño events. Figure 8 shows temporal evolutions of the MSE anomalies averaged over the western Pacific (5°–15°S, 120°–170°E, green box in Fig. 3). A positive MSE tendency is detected during the initiation and development stages of the MJO convection (Fig. 8a), when the OLR anomaly shows a negative tendency from day –20 to 0 (Fig. 5a). For the 2015/16 super El Niño event, the MSE tendency is larger than the other two events during the MJO initiation and development stages, resulting in enhanced MSE given the same time period for MJO development (from day –20 to 0), corresponding to the much stronger MJO activity. Evolutions of each column-integrated MSE budget term are displayed in Fig. 9 to inspect their respective contribution. The column-integrated MSE tendency $(\partial m/\partial t)'$ reaches the peak around day –10 (Fig. 9a), consistent with the moisture tendency (Fig. 5b). In comparison, the vertically integrated horizontal MSE advection resembles the phase evolution of the MSE tendency and can well explain the amplitude differ-

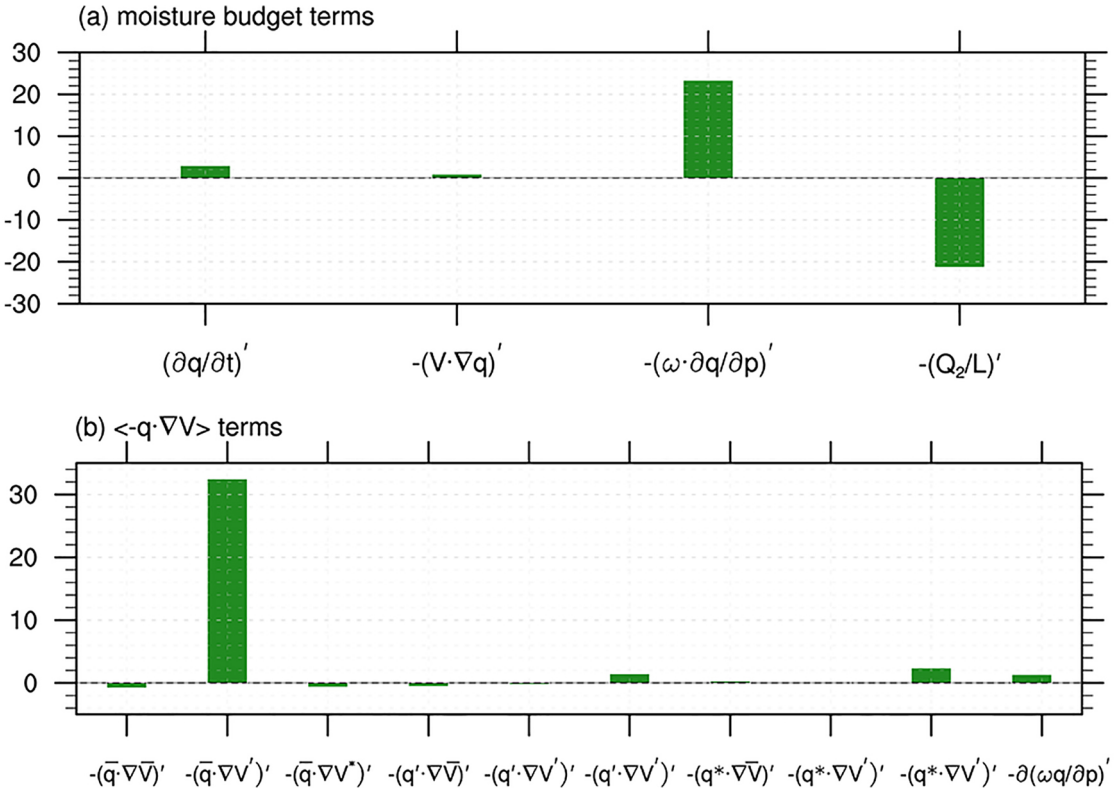

Fig. 6. Difference in lower troposphere (1000–700 hPa) column-integrated (a) intraseasonal moisture budget terms (10^{-6} kg m^{-2} s^{-1}) and (b) individual decomposition terms of $(V\partial q/\partial p)'$ between the boreal winter of 2015/16 and the average of the boreal winters of 1982/83 and 1997/98 over the western tropical Pacific (120°–170°E, 5°–15°S) from day –10 to day 0.

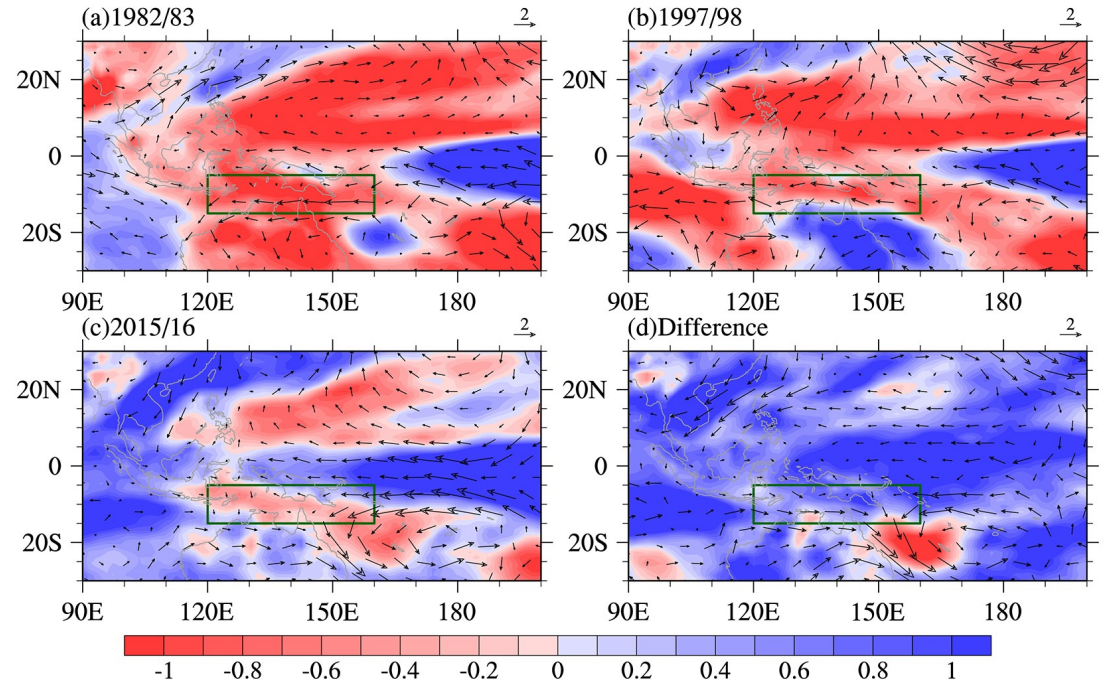

Fig. 7. Vertically averaged (1000–700 hPa) LFBS moisture (shading, g kg^{-1}) and MJO-related horizontal wind (vectors, m s^{-1}) anomalies for (a) 1982/83, (b) 1997/98, (c) 2015/16 and (d) difference between 2015/16 and the average of 1982/83 and 1997/98 from day –10 to day 0. The green boxes denotes the western tropical Pacific (5°–15°S, 120°–170°E).

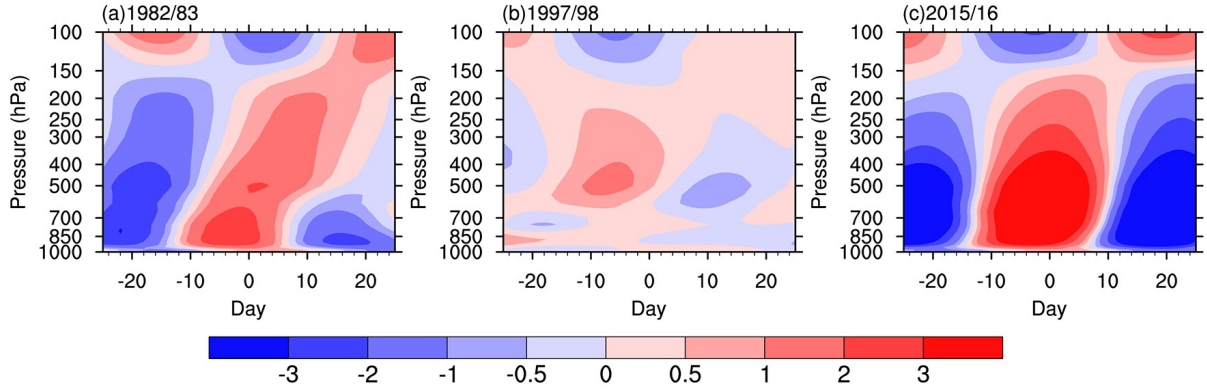

Fig. 8. Evolutions of intraseasonal MSE anomalies (kJ kg^{-1}) over the western Pacific (120°–170°E, 5°S–15°S) during the boreal winters of (a) 1982/83, (b) 1997/98, and (c) 2015/16. Note the day 0 represents the date of maximum MJO convection.

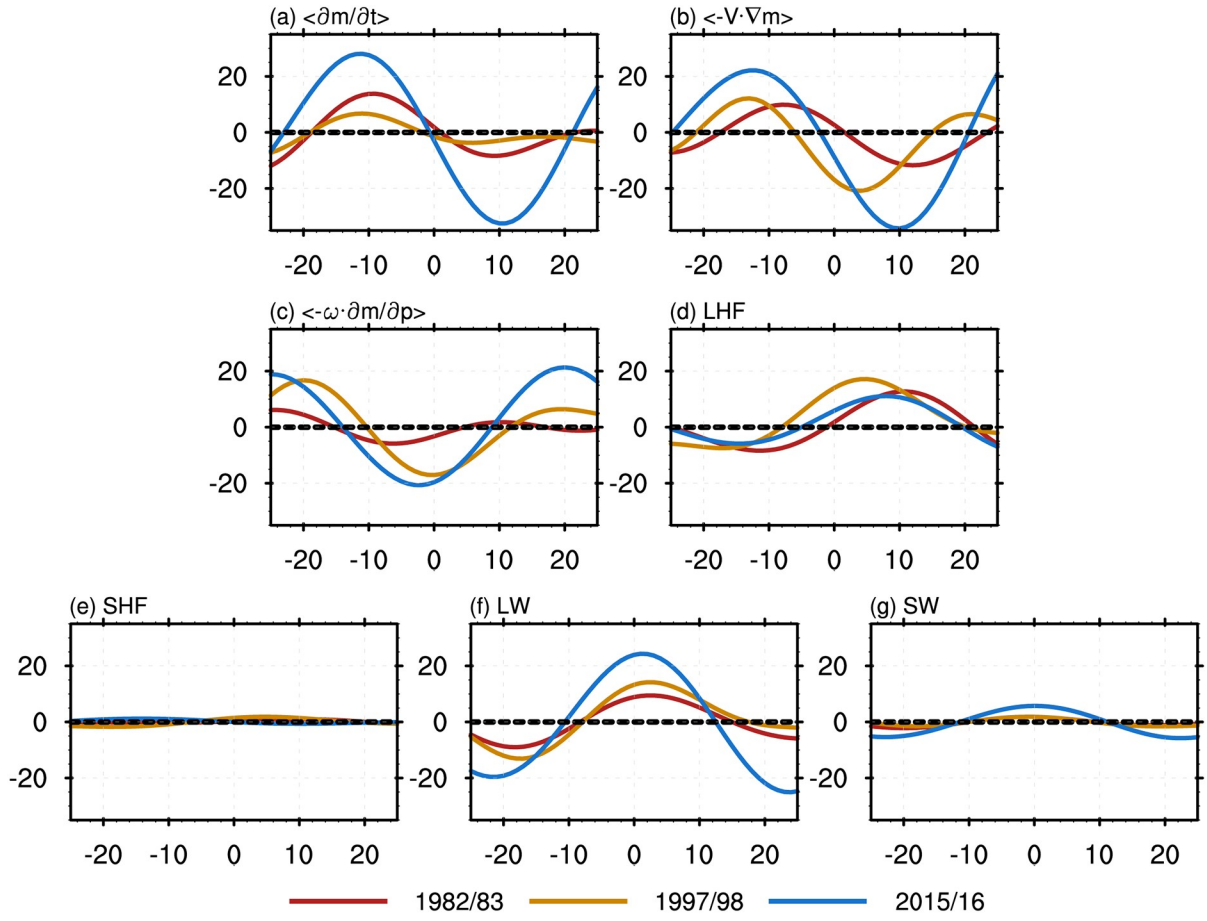

Fig. 9. Temporal evolutions of the column-integrated (1000–100 hPa) intraseasonal MSE budget terms (W m^{-2}) during the boreal winters of 1982/83 (red line), 1997/98 (orange line), and 2015/16 (blue line) over the western Pacific region (120°–170°E, 5°–15°S). Day 0 denotes the date of the maximum MJO convection.

ence for the three events (Fig. 9b), suggesting its important contribution to the differences in MJO activity. The column vertical MSE advection shifts its phase by about a quarter period respective to the MSE tendency and displays comparable amplitudes for the 1997/98 and 2015/16 events (Figs. 9c). The surface turbulent fluxes (Figs. 9d, e) and shortwave radiation (Fig. 9g) seem to have a minor contribution to the different MSE tendency. The evolution of longwave radiation (Fig. 9f) is in phase with the evolution of MJO convection. The amplitude of longwave radiation in the boreal winter of 2015/16 is larger than the other two events, indicating that the longwave radiation may maintain the stronger MJO convection in 2015/16 (Fig. 9f). The role of longwave radiation in supporting the MJO convection was highlighted by

previous studies (Andersen and Kuang, 2012; Maloney and Wolding, 2015; Hsu and Xiao, 2017).

For a purely quantitative comparison, we show the changes in amplitude of each budget term over the western Pacific during the initiation and development stages of the MJO convection (from day −20 to day 0). The differences in the MSE budget terms between the 2015/16 super El Niño and the other two super El Niño events are displayed in Fig. 10a. Note that the sum of the right-hand side terms is approximate to the left-hand side term (i.e., the MSE tendency), suggesting that our calculations are nearly balanced. The growth rate of MSE $(\partial m/\partial t)'$ during the 2015/16 super El Niño event is much larger than those during the 1982/83 and 1997/98 super El Niño events, consistent with the enhanced MJO activity. The horizontal advection here is the most dominant term for the growth rate of the MSE. In addition, the longwave radiation during the 2015/16 El Niño event is the secondary contributor for the growth of the MSE, and the larger longwave radiation has more positive feedback for the MJO convection, since increased cloudiness could produce larger longwave radiation. The other terms are relatively small and play minor roles on the MSE tendency. The MSE diagnostic results indicate that the horizontal advection of MSE is the key process inducing the enhancement of MJO convection during the 2015/16 super El Niño event. We next examine relative contributions of processes from different time-scale interactions to the horizontal MSE advection based on the following equation:

$$\begin{aligned} \mathrm{V}\cdot\nabla m = &\overline{V}\cdot\nabla\overline{m} + \overline{V}\cdot\nabla m' + \overline{V}\cdot\nabla m^* + \\ &V'\cdot\nabla\overline{m} + V'\cdot\nabla m' + V'\cdot\nabla m^* + \\ &V^*\cdot\nabla\overline{m} + V^*\cdot\nabla m' + V^*\cdot\nabla m^* . \end{aligned} \tag{6}$$

The decomposition of different time-scale interactions is the same as with Eqs. (4–5). As shown in Fig. 10b, the increased horizontal MSE advection in the 2015/16 super El Niño event is mostly attributable to the strengthened horizontal advection of the LFBS MSE by MJO-related horizontal wind. This result highlights the importance of interaction between the LFBS MSE and the MJO-related horizontal wind anomalies, as also revealed from the low-level moisture diagnosis (Figs. 6b, 7c). Figure 11 displays the vertically (1000–100 hPa) averaged distributions of LFBS MSE and intraseasonal horizontal wind anomalies. The boreal winters of 1982/83 and 1997/98 show negative LBFS MSE anomalies over the western Pacific (Figs. 11a, b), which are related to the below average SST anomalies (C_pT)

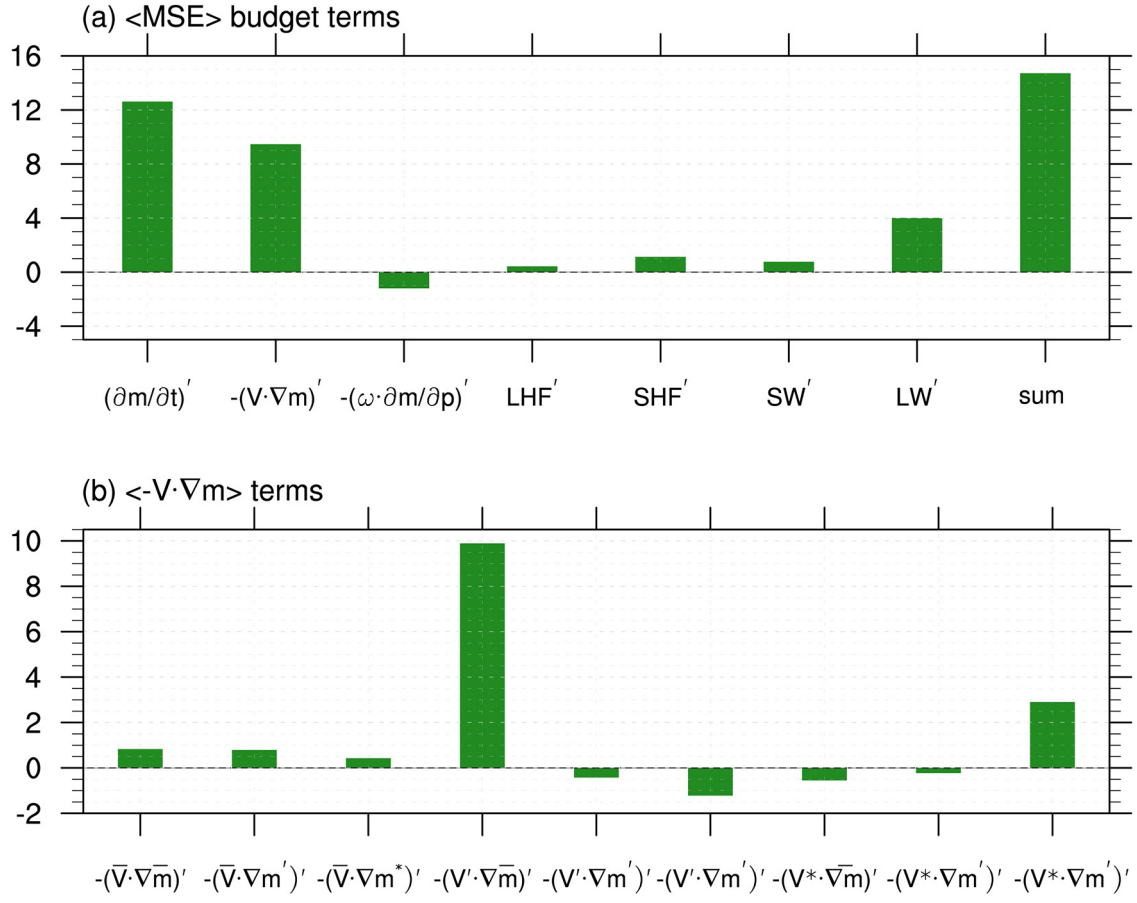

Fig. 10. Differences of column-integrated (1000–100 hPa) intraseasonal (a) MSE budget terms (W m^{-2}) and (b) individual terms of $(\mathrm{V}\cdot\nabla\mathrm{m})'$ averaged over the western Pacific region (120°–170°E, 5°–15°S) at the initiating and developing stages of MJO convection (from day −20 to day 0) between 2015/16 and the average of 1982/83 and 1997/98.

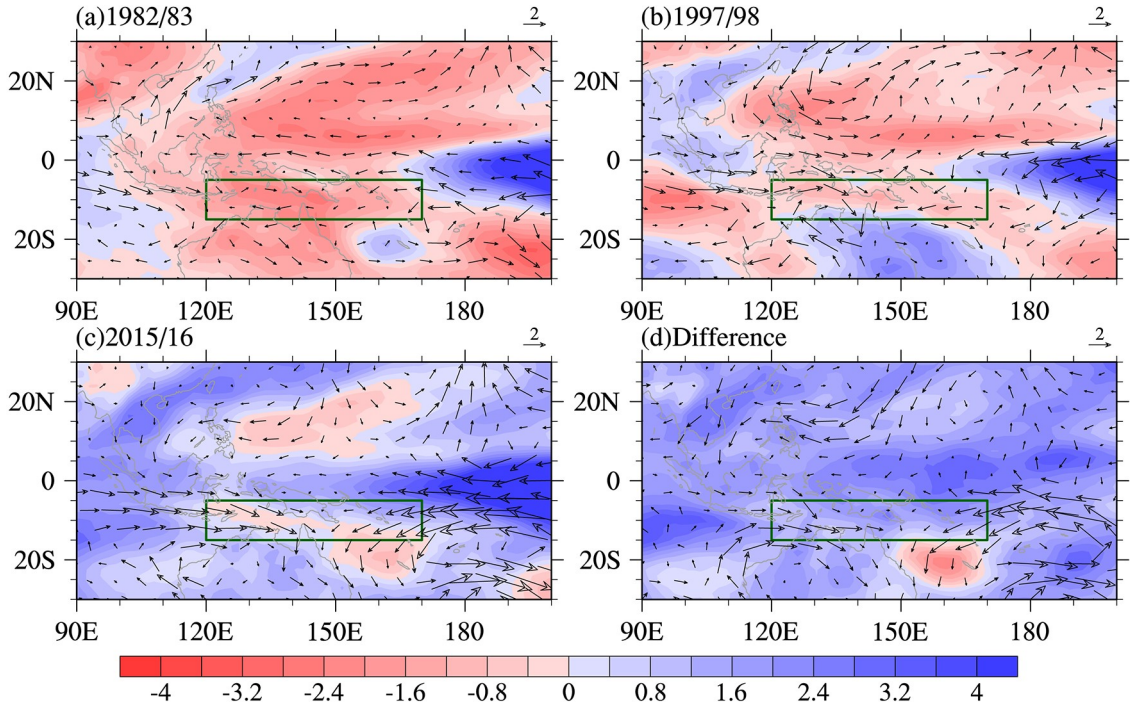

Fig. 11. Vertically averaged (1000–100 hPa) LFBS MSE anomalies (shading, 1×10^3 J kg^{-1}) and low-level (1000–700 hPa) MJO-related zonal wind anomalies (vectors, m s^{-1}) for (a) 1982/1983, (b) 1997/1998, (c) 2015/2016, and (d) difference between 2015/16 and the average of 1982/83 and 1997/98 from day −20 to day 0. The green boxes denote the western tropical Pacific (5°–15°S, 120°–170°E).

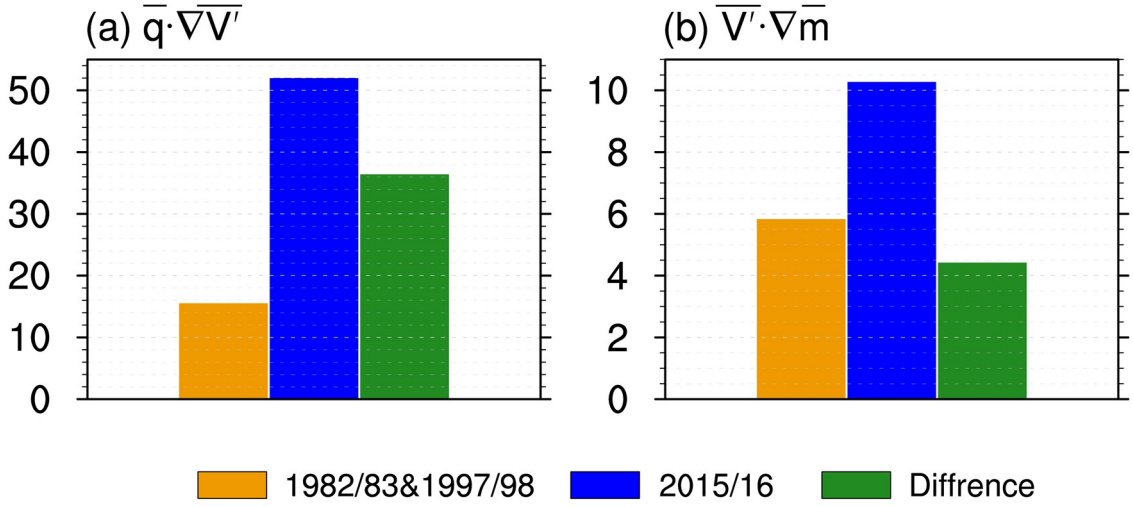

Fig. 12. Column-integrated intraseasonal (a) $\bar{q}\cdot\nabla\overline{V'}$ term (1000–700 hPa, g kg^{-1}) and (b) $\bar{V'}\cdot\nabla\overline{m}$ term (1000–100 hPa, W m^{-2}, where $\overline{V'}$ represents the averaged V' at the MJO developed stage during boreal winters of 1979–2018.

(Figs. 4a, b) and the below average moisture (Lq) (Figs. 7a, b). In contrast, the LBFS MSE is increased over the western equatorial Pacific during boreal winter of the 2015/16 super El Niño (Fig 11c), which is closely related to the westward displacement of the warm SSTAs and convection (Fig. 4c). The MJO-related wind anomalies tend to transport the relatively higher MSE toward the western Pacific, causing the increased MSE over the active MJO region (Figs. 11c and d). The MSE diagnostic results suggest that the warmer SSTs and thus low-level moistening during the 2015/16 super El Niño event could be the key factors responsible for the stronger MJO through enhancing the MSE over the western Pacific.

In the above analyses, the intraseasonal wind difference is accompanied with the MJO itself. It is not easy to establish a direct relationship between the MJO-related and ENSO-related variability, although the intraseasonal variability can be modulated by the background state. To illustrate direct contribution of the LFBS fields ($\bar{q}$ and $\bar{m}$) relatively, we use the averaged intraseasonal horizontal wind ($\bar{V'}$) from

1979 to 2018 during the MJO development stage to replace the $\overline{q}\cdot\nabla\overline{V'}$ and $\bar{V}'\cdot\nabla\overline{m}$ budgets over the western tropical Pacific (120°–170°E, 5°–15°S). Even though the MJO wind anomalies do not make a contribution, the $\overline{q}\cdot\nabla\overline{V'}$ and $\bar{V}'\cdot\nabla\overline{m}$ terms are apparently enhanced during the 2015/16 event compared to the 1982/83 and 1997/98 events (Fig. 12). Relative to the previous two events, the $\overline{q}\cdot\nabla\overline{V'}$ and $\bar{V}'\cdot\nabla\overline{m}$ terms are increased by 247% and 76%, respectively. Therefore, the moisture and MSE tendency can be enhanced by different background moisture patterns.

5. Conclusion and discussion

Previous observation shows that western Pacific MJO activity is strongly suppressed during the mature and decaying phases of super El Niño events (e.g., 1982/83 and 1997/98 El Niño events). The SSTAs of the most recent super El Niño event (i.e., 2015/16) also exhibit a very similar evolution and amplitude as the previous super El Niño events. However, this super El Niño event is accompanied by very different MJO activity with enhanced convection over the western Pacific during its peak phase. Compared to the 1982/83 and 1997/98 super El Niño events, the SSTA center during the 2015/16 super El Niño event shifts westward by about 20 degrees of longitude, which can provide sufficient moisture/MSE for MJO development over the western Pacific. The low-level moisture budget shows that vertical moisture advection is the major contributor to the enhancement of the MJO in 2015/16. This intensified vertical advection could be attributed to the interaction between the enhanced MJO-related zonal wind and the abundant low-frequency background moisture field over the central-western Pacific. The column-integrated MSE budget also suggests the interaction between MJO zonal wind anomalies and the background MSE field plays a key role in the enhancement of the MJO during the boreal winter of 2015/16. In other words, the increases in background moisture and MSE associated with the warm SSTAs over the central-western Pacific in the 2015/16 super El Niño event were important for the enhanced MJO activity.

Previous studies have revealed different MJO features, in terms of intensity and propagation, for the eastern Pacific (EP) and central Pacific (CP) El Niño. The MJO intensity and El Niño amplitude exhibit a certain degree of linear relationship for the EP and CP El Niño, respectively (Gushchina and Dewitte, 2012; Feng et al., 2015; Chen et al., 2016; Hsu and Xiao, 2017; Wang et al., 2018). Our study finds that MJO intensity is very sensitive to SSTA zonal location of El Niño, even the super El Niño (usually regarded as a same type) events have different impact. It highlights that the ENSO zonal structure and SSTA distribution need to be considered due to their possible modulations on MJO development. Only three super El Niño events are investigated to observe their differences in this study. However, to which extent the normal El Niño spatial SSTA patterns modulate on MJO development remains unclear and deserves further investigation.

Acknowledgements. This work was supported by the National Key R&D Program of China (2018YFC1505804), and the National Nature Science Foundation of China (42088101).

REFERENCES

Adames, Á. F., and J. M. Wallace, 2014: Three-dimensional structure and evolution of the vertical velocity and divergence fields in the MJO. *J. Atmos. Sci.*, **71**, 4661–4681, https://doi.org/10.1175/JAS-D-14-0091.1.

Alexander, M. A., I. Bladé, M. Newman, J. R. Lanzante, N. C. Lau, and J. D. Scott, 2002: The atmospheric bridge: The influence of ENSO teleconnections on air-sea interaction over the global oceans. *J. Climate*, **15**, 2205–2231, https://doi.org/10.1175/1520-0442(2002)015<2205:TABTIO>2.0.CO;2.

Andersen, J. A., and Z. M. Kuang, 2012: Moist static energy budget of MJO-like disturbances in the atmosphere of a zonally symmetric aquaplanet. *J. Climate*, **25**, 2782–2804, https://doi.org/10.1175/JCLI-D-11-00168.1.

Ashok, K., C. Y. Tam, and W. J. Lee, 2009: ENSO Modoki impact on the Southern Hemisphere storm track activity during extended austral winter. *Geophys. Res. Lett.*, **36**, L12705, https://doi.org/10.1029/2009GL038847.

Bjerknes, J., 1969: Atmospheric teleconnections from the equatorial Pacific. *Mon. Wea. Rev.*, **97**, 163–172, https://doi.org/10.1175/1520-0493(1969)097<0163:ATFTEP>2.3.CO;2.

Camargo, S. J., M. C. Wheeler, and A. H. Sobel, 2009: Diagnosis of the MJO modulation of tropical cyclogenesis using an empirical index. *J. Atmos. Sci.*, **66**, 3061–3074, https://doi.org/10.1175/2009JAS3101.1.

Cassou, C., 2008: Intraseasonal interaction between the Madden-Julian Oscillation and the North Atlantic Oscillation. *Nature*, **455**, 523–527, https://doi.org/10.1038/nature07286.

Chen, L., T. Li, B. Wang, and L. Wang, 2017: Formation Mechanism for 2015/16 Super El Niño. *Sci. Rep.*, **7**, 2975, https://doi.org/10.1038/s41598-017-02926-3.

Chen, X., C. Y. Li, and Y. K. Tan, 2015: The influence of El Niño on MJO over the equatorial pacific. *Journal of Ocean University of China*, **14**, 1–8, https://doi.org/10.1007/s11802-015-2381-y.

Chen, X., J. Ling, and C. Y. Li, 2016: Evolution of the Madden-Julian oscillation in two types of El Niño. *J. Climate*, **29**, 1919–1934, https://doi.org/10.1175/JCLI-D-15-0486.1.

Dee, D. P., and Coauthors, 2011: The ERA-interim reanalysis: Configuration and performance of the data assimilation system. *Quart. J. Roy. Meteor. Soc.*, **137**, 553–597, https://doi.org/10.1002/qj.828.

Duchon, C. E., 1979: Lanczos filtering in one and two dimensions. *J. Appl. Meteorol. Climatol.*, **18**, 1016–1022, https://doi.org/10.1175/1520-0450(1979)018<1016:LFIOAT>2.0.CO;2.

Feng, J., P. Liu, W. Chen, and X. C. Wang, 2015: Contrasting Madden-Julian oscillation activity during various stages of ep and CP El Niños. *Atmospheric Science Letters*, **16**, 32–37, https://doi.org/10.1002/asl2.516.

Ferranti, L., T. N. Palmer, F. Molteni, and E. Klinker, 1990: Tropical-extratropical interaction associated with the 30–60 day oscillation and its impact on medium and extended range prediction. *J. Atmos. Sci.*, **47**, 2177–2199, https://doi.org/10.

1175/1520-0469(1990)047<2177:TEIAWT>2.0.CO;2.

Geng, X., W. J. Zhang, M. F. Stuecker, P. Liu, F. F. Jin, and G. R. Tan, 2017: Decadal modulation of the ENSO-East Asian winter monsoon relationship by the Atlantic Multidecadal Oscillation. *Climate Dyn.*, **49**, 2531–2544, https://doi.org/10.1007/s00382-016-3465-0.

Gushchina, D., and B. Dewitte, 2012: Intraseasonal tropical atmospheric variability associated with the two flavors of El Niño. *Mon. Wea. Rev.*, **140**, 3669–3681, https://doi.org/10.1175/MWR-D-11-00267.1.

Hendon, H. H., M. C. Wheeler, and C. D. Zhang, 2007: Seasonal dependence of the MJO-ENSO relationship. *J. Climate*, **20**, 531–543, https://doi.org/10.1175/JCLI4003.1.

Hsu, P. C., and T. Li, 2012: Role of the boundary layer moisture asymmetry in causing the eastward propagation of the Madden-Julian oscillation. *J. Climate*, **25**, 4914–4931, https://doi.org/10.1175/JCLI-D-11-00310.1.

Hsu, P. C., and T. Xiao, 2017: Differences in the initiation and development of the Madden-Julian oscillation over the Indian Ocean associated with two types of El Niño. *J. Climate*, **30**, 1397–1415, https://doi.org/10.1175/JCLI-D-16-0336.1.

Jacox, M. G., E. L. Hazen, K. D. Zaba, D. L. Rudnick, C. A. Edwards, A. M. Moore, and S. J. Bograd, 2016: Impacts of the 2015–2016 El Niño on the California Current System: Early assessment and comparison to past events. *Geophys. Res. Lett.*, **43**, 7072–7080, https://doi.org/10.1002/2016GL069716.

Kao, H. Y., and J. Y. Yu, 2009: Contrasting Eastern-Pacific and central-pacific types of ENSO. *J. Climate*, **22**, 615–632, https://doi.org/10.1175/2008JCLI2309.1.

Kapur, A., and C. D. Zhang, 2012: Multiplicative MJO forcing of ENSO. *J. Climate*, **25**, 8132–8147, https://doi.org/10.1175/JCLI-D-11-00609.1.

Kemball-Cook, S. R., and B. C. Weare, 2001: The onset of convection in the Madden-Julian oscillation. *J. Climate*, **14**, 780–793, https://doi.org/10.1175/1520-0442(2001)014<0780:TOOCIT>2.0.CO;2.

Kessler, W. S., M. J. McPhaden, and K. M. Weickmann, 1995: Forcing of intraseasonal Kelvin waves in the equatorial Pacific. *J. Geophys. Res.*, **100**, 10613–10631, https://doi.org/10.1029/95JC00382.

Kiladis, G. N., K. H. Straub, and P. T. Haertel, 2005: Zonal and vertical structure of the Madden-Julian oscillation. *J. Atmos. Sci.*, **62**, 2790–2809, https://doi.org/10.1175/JAS3520.1.

Kim, D., J. S. Kug, and A. H. Sobel, 2014: Propagating versus nonpropagating Madden-Julian oscillation events. *J. Climate*, **27**, 111–125, https://doi.org/10.1175/JCLI-D-13-00084.1.

Kim, H. M., C. D. Hoyos, P. J. Webster, and I. S. Kang, 2010: Ocean-atmosphere coupling and the boreal winter MJO. *Climate Dyn.*, **35**, 771–784, https://doi.org/10.1007/s00382-009-0612-x.

Kug, J. S., F. F. Jin, and S. I. An, 2009: Two types of El Niño events: Cold tongue El Niño and warm pool El Niño. *J. Climate*, **22**, 1499–1515, https://doi.org/10.1175/2008JCLI2624.1.

L'Heureux, M. L., and Coauthors, 2017: Observing and Predicting the 2015/16 El Niño. *Bull. Amer. Meteor. Soc.*, **98**, 1363–1382, https://doi.org/10.1175/BAMS-D-16-0009.1.

Larkin, N. K., and D. E. Harrison, 2005: Global seasonal temperature and precipitation anomalies during El Niño autumn and winter. *Geophys. Res. Lett.*, **32**, L16705, https://doi.org/10.1029/2005GL022860.

Lau, N. C., and M. J. Nath, 2006: ENSO modulation of the interannual and intraseasonal variability of the East Asian monsoon–A model study. *J. Climate*, **19**, 4508–4530, https://doi.org/10.1175/JCLI3878.1.

Levine, A. F. Z., and M. J. McPhaden, 2016: How the July 2014 easterly wind burst gave the 2015-2016 El Niño a head start. *Geophys. Res. Lett.*, **43**, 6503–6510, https://doi.org/10.1002/2016GL069204.

Li, K. P., Y. L. Liu, Z. Li, Y. Yang, L. Feng, S. Khokiattiwong, W. D. Yu, and S. H. Liu, 2018: Impacts of ENSO on the Bay of Bengal summer monsoon onset via modulating the intraseasonal oscillation. *Geophys. Res. Lett.*, **45**, 5220–5228, https://doi.org/10.1029/2018GL078109.

Liebmann, B., and C. A. Smith, 1996: Description of a complete (interpolated) outgoing longwave radiation dataset. *Bull. Amer. Meteor. Soc.*, **77**, 1275–1277.

Liebmann, B., H. H. Hendon, and J. D. Glick, 1994: The relationship between tropical cyclones of the western Pacific and Indian Oceans and the Madden-Julian oscillation. *J. Meteor. Soc. Japan*, **72**, 401–412, https://doi.org/10.2151/jmsj1965.72.3_401.

Lin, A. L., and T. Li, 2008: Energy spectrum characteristics of boreal summer intraseasonal oscillations: Climatology and variations during the ENSO developing and decaying phases. *J. Climate*, **21**, 6304–6320, https://doi.org/10.1175/2008JCLI2331.1.

Liu, F., T. Li, H. Wang, L. Deng, and Y. W. Zhang, 2016a: Modulation of boreal summer intraseasonal oscillations over the western North Pacific by ENSO. *J. Climate*, **29**, 7189–7201, https://doi.org/10.1175/JCLI-D-15-0831.1.

Liu, F., L. Zhou, J. Ling, X. H. Fu, and G. Huang, 2016b: Relationship between SST anomalies and the intensity of intraseasonal variability. *Theor. Appl. Climatol.*, **124**(3–4), 847–854, https://doi.org/10.1007/s00704-015-1458-2.

Lyu, Y., Y. L. Li, X. H. Tang, F. Wang, and J. N. Wang, 2018: Contrasting intraseasonal variations of the equatorial pacific ocean between the 1997–1998 and 2015–2016 El Niño events. *Geophys. Res. Lett.*, **45**, 9748–9756, https://doi.org/10.1029/2018GL078915.

Madden, R. A., and P. R. Julian, 1971: Detection of a 40–50 day oscillation in the zonal wind in the tropical Pacific. *J. Atmos. Sci.*, **28**, 702–708, https://doi.org/10.1175/1520-0469(1971)028<0702:DOADOI>2.0.CO;2.

Madden, R. A., and P. R. Julian, 1972: Description of global-scale circulation cells in the tropics with a 40-50 day period. *J. Atmos. Sci.*, **29**, 1109–1123, https://doi.org/10.1175/1520-0469(1972)029<1109:DOGSCC>2.0.CO;2.

Maloney, E. D., 2009: The moist static energy budget of a composite tropical intraseasonal oscillation in a climate model. *J. Climate*, **22**, 711–729, https://doi.org/10.1175/2008JCLI2542.1.

Maloney, E. D., and B. O. Wolding, 2015: Initiation of an intraseasonal oscillation in an aquaplanet general circulation model. *Journal of Advances in Modeling Earth Systems*, **7**, 1956–1976, https://doi.org/10.1002/2015MS000495.

McPhaden, M. J., 1999: Genesis and evolution of the 1997–98 El Niño. *Science*, **283**, 950–954, https://doi.org/10.1126/science.283.5404.950.

Neelin, J. D., and I. M. Held, 1987: Modeling tropical convergence based on the moist static energy budget. *Mon. Wea. Rev.*, **115**, 3–12, https://doi.org/10.1175/1520-0493(1987)

115<0003:MTCBOT>2.0.CO;2.

Paek, H., J. Y. Yu, and C. C. Qian, 2017: Why were the 2015/2016 and 1997/1998 extreme El Niños different? Geophys *Res. Lett.*, **44**, 1848–1856, https://doi.org/10.1002/2016GL071515.

Pritchard, M. S., and C. S. Bretherton, 2014: Causal evidence that rotational moisture advection is critical to the superparameterized Madden-Julian oscillation. *J. Atmos. Sci.*, **71**, 800–815, https://doi.org/10.1175/JAS-D-13-0119.1.

Rayner, N. A., D. E. Parker, E. B. Horton, C. K. Folland, L. V. Alexander, D. P. Rowell, E. C. Kent, and A. Kaplan, 2003: Global analyses of sea surface temperature, sea ice, and night marine air temperature since the late nineteenth century. *J. Geophys. Res.*, **108**, 4407, https://doi.org/10.1029/2002JD002670.

Ren, H. L., and F. F. Jin, 2011: Niño indices for two types of ENSO. *Geophys. Res. Lett.*, **38**, L04704, https://doi.org/10.1029/2010GL046031.

Smith, S. R., D. M. Legler, M. J. Remigio, and J. J. O'Brien, 1999: Comparison of 1997–98 U.S. temperature and precipitation anomalies to historical ENSO warm phases. *J. Climate*, **12**, 3507–3515, https://doi.org/10.1175/1520-0442(1999)012<3507:COUSTA>2.0.CO;2.

Sobel, A., and E. Maloney, 2013: Moisture modes and the eastward propagation of the MJO. *J. Atmos. Sci.*, **70**, 187–192, https://doi.org/10.1175/JAS-D-12-0189.1.

Sperber, K. R., 2003: Propagation and the vertical structure of the Madden-Julian oscillation. *Mon. Wea. Rev.*, **131**, 3018–3037, https://doi.org/10.1175/1520-0493(2003)131<3018:PATVSO>2.0.CO;2.

Tang, Y. M., and B. Yu, 2008: MJO and its relationship to ENSO. *J. Geophys. Res.*, **113**, D14106, https://doi.org/10.1029/2007JD009230.

Vecchi, G. A., and D. E. Harrison, 2000: Tropical Pacific Sea surface temperature anomalies, El Niño, and equatorial westerly wind events. *J. Climate*, **13**, 1814–1830, https://doi.org/10.1175/1520-0442(2000)013<1814:TPSSTA>2.0.CO;2.

Wallace, J. M., E. M. Rasmusson, T. P. Mitchell, V. E. Kousky, E. S. Sarachik, and H. Von Storch, 1998: On the structure and evolution of ENSO-related climate variability in the tropical Pacific: Lessons from TOGA. *J. Geophys. Res.*, **103**, 14241–14259, https://doi.org/10.1029/97JC02905.

Wang, B., 1988: Dynamics of tropical low-frequency waves—An analysis of the moist Kelvin wave. *J. Atmosp.heric Sci.*, **45**, 2051–2065, https://doi.org/10.1175/1520-0469(1988)045<2051:DOTLFW>2.0.CO;2.

Wang, B., G. S. Chen, and F. Liu, 2019: Diversity of the Madden-Julian oscillation. *Science Advances*, **5**(7), eaax0220, https://doi.org/10.1126/sciadv.aax0220.

Wang, L., T. Li, L. Chen, S. K. Behera, and T. Nasuno, 2018: Modulation of the MJO intensity over the equatorial western Pacific by two types of El Niño. *Climate Dyn.*, **51**, 687–700, https://doi.org/10.1007/s00382-017-3949-6.

Weickmann, K. M., G. R. Lussky, and J. E. Kutzbach, 1985: Intraseasonal (30–60 day) fluctuations of outgoing longwave radiation and 250 mb streamfunction during Northern Winter. *Mon. Wea. Rev.*, **113**, 941–961, https://doi.org/10.1175/1520-0493(1985)113<0941:IDFOOL>2.0.CO;2.

Wheeler, M. C., and H. H. Hendon, 2004: An all-season real-time multivariate MJO index: Development of an index for monitoring and prediction. *Mon. Wea. Rev.*, **132**, 1917–1932, https://doi.org/10.1175/1520-0493(2004)132<1917:AARMMI>2.0.CO;2.

Xie, P. P., and P. A. Arkin, 1997: Global precipitation: A 17-year monthly analysis based on gauge observations, satellite estimates, and numerical model outputs. *Bull. Amer. Meteor. Soc.*, **78**, 2539–2558, https://doi.org/10.1175/1520-0477(1997)078<2539:GPAYMA>2.0.CO;2.

Yanai, M., S. Esbensen, and J. H. Chu, 1973: Determination of bulk properties of tropical cloud clusters from large-scale heat and moisture budgets. *J. Atmos. Sci.*, **30**, 611–627, https://doi.org/10.1175/1520-0469(1973)030<0611:DOBPOT>2.0.CO;2.

Yasunari, T., 1979: Cloudiness fluctuations associated with the Northern Hemisphere summer monsoon. *J. Meteor. Soc. Japan*, **57**(3), 227–242, https://doi.org/10.2151/jmsj1965.57.3_227.

Zavala-Garay, J., C. Zhang, A. M. Moore, and R. Kleeman, 2005: The linear response of ENSO to the Madden-Julian oscillation. *J. Climate*, **18**, 2441–2459, https://doi.org/10.1175/JCLI3408.1.

Zhang, C. D., and J. Gottschalck, 2002: SST Anomalies of ENSO and the Madden-Julian Oscillation in the Equatorial Pacific. *J. Climate*, **15**, 2429–2445, https://doi.org/10.1175/1520-0442(2002)015<2429:SAOEAT>2.0.CO;2.

Zhang, W. J., F. F. Jin, and A. Turner, 2014: Increasing autumn drought over southern China associated with ENSO regime shift. *Geophys. Res. Lett.*, **41**, 4020–4026, https://doi.org/10.1002/2014GL060130.

Zhang, W. J., and Coauthors, 2016: Unraveling El Niño's impact on the East Asian monsoon and Yangtze River summer flooding. *Geophys. Res. Lett.*, **43**(21), 11375–11382, https://doi.org/10.1002/2016GL071190.

Zhang, W. J., H. Y. Li, F. F. Jin, M. F. Stuecker, A. G. Turner, and N. P. Klingaman, 2015: The annual-cycle modulation of meridional asymmetry in ENSO's atmospheric response and its dependence on ENSO zonal structure. *J. Climate*, **28**, 5795–5812, https://doi.org/10.1175/JCLI-D-14-00724.1.

Zhao, C. B., T. Li, and T. J. Zhou, 2013: Precursor signals and processes associated with MJO initiation over the tropical Indian Ocean. *J. Climate*, **26**, 291–307, https://doi.org/10.1175/JCLI-D-12-00113.1.

Zheng, C., E. K. M. Chang, H. M. Kim, M. H. Zhang, and W. Q. Wang, 2018: Impacts of the Madden-Julian oscillation on storm-track activity, surface air temperature, and precipitation over North America. *J. Climate*, **31**, 6113–6134, https://doi.org/10.1175/JCLI-D-17-0534.1.